Gap-Filling of Turbulent Heat Fluxes over Rice–Wheat-Rotation Croplands Using the Random Forest Model

Jianbin Zhang[1], Zexia Duan[1], Shaohui Zhou[1], Yubin Li[1], Zhiqiu Gao[1]

[1] School of Atmospheric Physics, Nanjing University of Information Science & Technology, Nanjing, 210044, China

Correspondence to: Dr. Yubin Li (liyubin@nuist.edu.cn)

Abstract. This study investigated the accuracy of the Random Forest (RF) model in gap-filling the sensible (H) and latent heat (LE) fluxes, by using the observation data collected at a site over rice–wheat-rotation croplands in Shouxian County of eastern China from 15 July 2015 to 24 April 2019. Firstly, the variable significances of the machine learning (ML) model's five input variables, including the net radiation (Rn), winds speed (WS), temperature (T), relative humidity (RH), and air pressure (P), were examined, and it was found that Rn accounted for 78% and 76% of the total variable significance in H and LE calculating, respectively, showing that it was the most important input variable. Secondly, the RF model's accuracy with the five-variable (Rn, WS, T, RH, P) input combination was evaluated, and the results showed that the RF model could reliably gap-fill the H and LE with mean absolute errors (MAEs) of 5.88 Wm^{-2} and 20.97 Wm^{-2}, and root mean square errors (RMSEs) of 10.67 Wm^{-2} and 29.46 Wm^{-2}, respectively. Thirdly, 4-variable input combinations were tested, and it was found that the best input combination was (Rn, WS, T, P) by removing RH from the input list, and its MAE values of H and LE were reduced by 12.65% and 7.12%, respectively. At last, through the Taylor diagram, H and LE gap-filling accuracies of the RF model, the support vector machine (SVM) model, the k-nearest neighbor (KNN) model, and the gradient boosting decision tree (GBDT) model were inter-compared, and the statistical metrics showed that RF was the most accurate for both H and LE gap-filling, while the LR and KNN model performed the worst for H and LE gap-filling, respectively.

1 Introduction

The turbulent fluxes between the atmosphere and the ground play a crucial role in global climate change and atmospheric circulation, and the inaccuracy of long-term observations of surface turbulent fluxes is a major factor in erroneous weather predictions and climate projections. Research on the ecological effects of urban green spaces, agricultural ecosystems, and forests all use surface turbulent fluxes as key indicators. Currently, the eddy covariance (EC) technique can be used to directly measure the turbulent fluxes (Wilson et al., 2001; Jiang et al., 2021; Wang et al., 2021). However, due to sensor failure and adverse meteorological factors (such as rainfall and frost), these high-frequency turbulence data are subject to errors (Khan et al., 2018). As a result, it is difficult to obtain a continuous time series of ground-based turbulent fluxes. Furthermore, quality assurance methods lead to unavailable sections of flux datasets (Nisa et al., 2021). Based on the above reasons, gap-filling is in need to retrieve continuous datasets of EC-based fluxes. Researchers have developed approaches based on existing

31 meteorological information to fill up the gaps in atmospheric databases, such as interpolation, nonlinear regression, mean

32 diurnal method, and sampling techniques from the marginal distribution (Falge et al., 2001; Hui et al., 2004; Stauch et al.,

33 2006; Foltnov et al., 2020). Further, the ML technique has also become an effective method to be used in the calculation of

34 turbulent fluxes (McCandless et al., 2022).

35

36 As a result of recent developments in high computing technology, machine-learning-based algorithms have been developed

37 and successfully used in various areas, such as natural language processing, data mining, biometrics, computer vision, search

38 engines, clinical applications, video games, robots, etc. To address the missing data issue, machine-learning-based models

39 have recently been used to fill data gaps in meteorological elements and turbulent fluxes (Bianco et al., 2019; Yu et al., 2020).

40 As a result of their reliable and repeatable results, these models are now regarded as a standard gap-filling algorithm (Beringer

41 et al., 2017; Isaac et al., 2017). ML algorithms have several deficiencies even if they perform well in some areas. For instance,

42 over-fitting is a major concern that can occur when the training window is too short or the training dataset's quality is poor.

43 That's because the present ML approaches are not sufficiently adaptable to work in extreme situations with large values

44 (Kunwor et al., 2017; Moffat et al., 2007). Furthermore, even with the best technique, the model uncertainty of gap-filling still

45 plays a role, particularly when the gaps are relatively large. Numerous novel ML and optimization algorithms have been created

46 and put to use in numerous scientific domains since the 2000s, and their superiority has been demonstrated, either singly or as

47 a component of a hybrid or ensemble model (e.g. Gani et al., 2016).

48

49 Based on the need for fluxes dataset gap-filling, and the effectivity of the ML technique, this paper aims, firstly, to investigate

50 the performance of the RF machine learning algorithm trained from a dataset obtained over rice-wheat-rotation croplands in

51 Shouxian County, eastern China, in gap-filling the sensible and latent heat fluxes; and secondly, to analyze the RF model's

52 accuracy with various meteorological input combinations during training; and thirdly, to compare the performance of RF model

53 with other four typical ML models.

54

2 Materials and Methods

2.1 Study area

57 This observation was conducted at a site in Shouxian County in the eastern Chinese province of Anhui (32.42 °N, 116.76 °E)

58 (Figure 1). The altitude of the site is 27 meters, and the annual mean air temperature and annual cumulative precipitation here

59 are 16 °C and 1115 mm, respectively. Summer (from June to September) precipitation accounts for nearly 60% of the annual

60 precipitation amount, which meets the high water demand of rice. Drought sometimes occurs due to lack of precipitation in

61 the growing season of wheat. This observation site is rather flat, with farmland accounting for more than 90% of the area.

62 Winter wheat is grown here from November until late May, while from June to November the field is flooded, plowed, and

harrowed as rice paddies (Duan et al., 2021) (Figure 2). The subtropical northern boundary of the monsoon humid climatic type describes the area's climate.
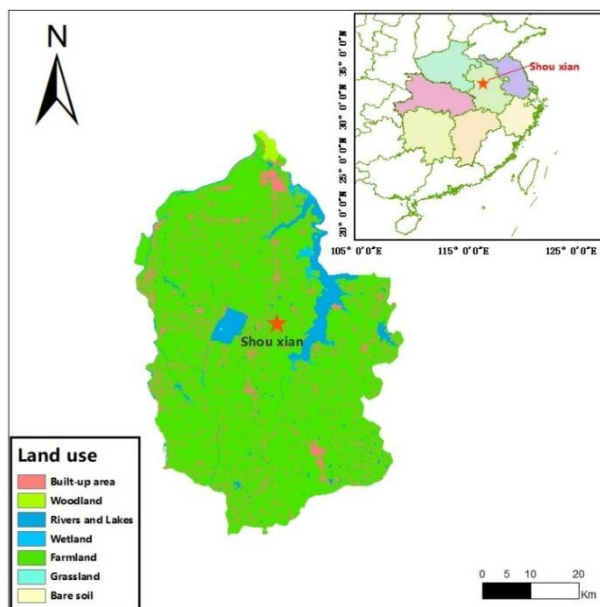
Figure 1. Geographical location and land-cover map of Shouxian County.
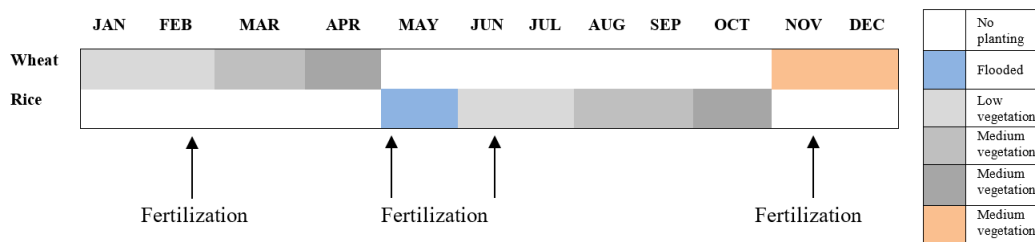
Figure 2. Crop calendars for the rice and wheat in the North Yangtze River Delta region.

2.2 Data

Over the site described above, EC sensors (EC 150, Campbell Scientific Inc., Logan, UT, USA) were installed at 2.5 meters above the ground, including a three-dimensional sonic anemometer (CSAT3, Campbell Scientific Inc., Logan, UT, USA) and a CO_2/H_2O open-path infrared gas analyzer. The sensible and latent heat fluxes were computed half-hourly using EddyPro

78 software, with time lag compensation, double coordinate rotation, spectrum correction, and Webb-Pearman-Leuning density

79 correction (Wutzler et al., 2018; Anapalli et al., 2019). Poor-quality fluxes (Eddypro quality check flag value=2) were

80 discarded. And a quality check based on the relationship between the measured flux and friction velocity was carried out to
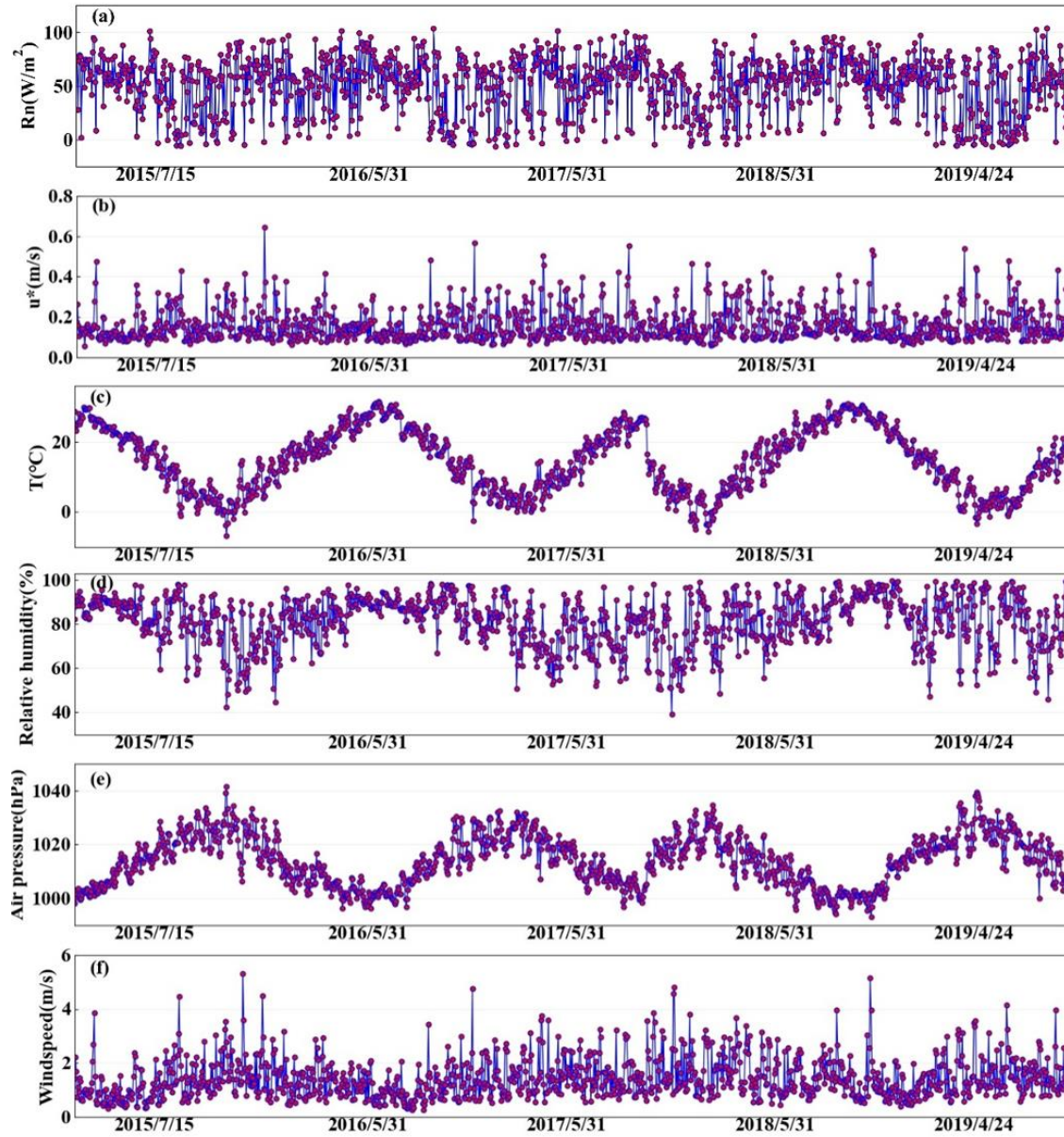
81

82

83 **Figure 3. Daily averaged a) Rn: net radiation(Wm⁻²) , b) u*: friction velocity(m/s), c) T: air temperature(°C), d) RH: relative**
84 **humidity(%), e) P: air pressure(hPa), and f) WS:wind speed(m s⁻¹).**

85

86   remove the biased data (Papale et al., 2006). Then, using the marginal distribution sampling technique, the flow data were gap-

87   filled (Reichstein et al., 2005). The time series of air temperature, relative humidity, wind speed, air pressure, friction velocity,

88   and net radiation were also subjected to quality control. The missing data which need gapfilling are H and LE, with 7205 and

89   16013 missing, accounting for 12.09% and 26.87% respectively. According to the criteria of $X(h) < (X - 4\sigma)$ or $X(h) > (X +$

90   $4\sigma)$, where $X(h)$ indicates the time series of the component, X is the mean across the averaging interval, and σ is the standard

91   deviation, noisy data were eliminated (Gao et al., 2003). Data observed from 15 July 2015 to 24 April 2019 are used in this

92   study, and Figure 3 shows the daily average data of Rn: net radiation(W m^{-2}), u*: friction velocity(m/s), T: air temperature(℃),

93   RH: relative humidity(%), P: air pressure(hPa), and WS: wind speed(m s^{-1}).

94

95   **2.3 The RF Model**

96   RF is a machine learning method that is quick, adaptable, and frequently used to analyze classification and regression jobs

97   (Breiman, 2001). This model can successfully evaluate highly dimensional and multicollinear data and is resistant to overfitting

98   (Belgiu et al., 2016). The RF model provides a feature-selection tool to assist in determining the importance of the predictor.

99   The contribution of each variable to the model, with important variables having a higher effect on the results of the model

100 evaluation, is the definition of feature significance (Liu et al., 2021). 90% of the data collected at the Shouxian observation

101 site throughout the study period were used to train the RF model, while the remaining 10% was used to independently validate

102 the model (hereafter, validation dataset). To lessen the overfitting in this case, a 10-fold cross-validation (CV) procedure was

103 used (Cai et al., 2020). All training data used here was randomly divided into ten subsamples of equal size for the 10-fold CV

104 tests. And nine out of the ten subsamples were used as training data (hereafter, training dataset), while the remaining subsample

105 was used as testing data (hereafter, testing dataset). All ten of the subsamples were utilized as testing data exactly once for

106 each of the 10 iterations of the CV procedure. One estimate was created by averaging the 10 findings from the folds. We

107 modified the four RF model hyperparameters based on Bayesian optimization to get the optimal model (Baareh et al., 2021;

108 Frazier, P.I., 2018): the maximum number of features considered to split a node (Max features), the maximum number of trees

109 to build (n estimators), the minimum sample number placed in a node prior to the node being split (min split), and the maximum

110 number of levels for each decision tree (Max depth). Bayesian optimizer is used to tune parameters, you can quickly find an

111 acceptable hyperparameter value, compared with grid search, the advantage is that the number of iterations is less (time saving),

112 the granularity can be very small. For example, if we want to adjust the regularized hyperparameters of linear regression, we

113 set the black box function to linear regression, the independent variable is a hyperparameter, the dependent variable is linear

114 regression in the training set accuracy, set an acceptable black box function dependent variable value, such as 0.95, the obtained

115 hyperparameter result is a hyperparameter that can make the linear regression accuracy exceed 0.95. The simulated

116 performance of the 10-fold CV outcomes was evaluated using four statistical metrics: the correlation coefficient (*r*), mean

117 absolute error (MAE), root mean square error (RMSE), and standard deviation(σ_n). As a result, the final RF model's parameters

118 were adjusted to n estimators = 246, min split = 2, Max features = 10, and Max depth = 35, to have the best statistical metrics.

119 The four statistical metrics are calculated by:

$$r = \frac{\sum_{i=1}^{N}(S_i - \bar{S})(O_i - \bar{O})}{\sqrt{\sum_{i=1}^{N}(S_i - \bar{S})^2}\sqrt{\sum_{i=1}^{N}(O_i - \bar{O})^2}}, \qquad (1)$$

120

121

$$\text{MAE} = \frac{1}{N}\sum_{i=1}^{N}|S_i - O_i|, \qquad (2)$$

122

123

$$\text{RMSE} = \sqrt{\frac{\sum_{i=1}^{N}(S_i - O_i)^2}{N}}, \qquad (3)$$

124

125

$$\sigma_n = \frac{\sqrt{\sum_{i=1}^{N}(S_i - O_i)^2}}{N}. \qquad (4)$$

126

127

128 where S stands for the modeled value, O is the observation, $\bar{O}$ is the mean observed value, and $\bar{S}$ is the mean modeled

129 observation, σ_n indicates the standard deviation. The subscript i represents the serial number of samples, and N represents the

130 total number of samples.

131

132 **3 Results and discussion**

133 **3.1 Driving Factors of H and LE on a Seasonal Scale**

134 The possible driving factors of H and LE were investigated to determine their respective contributions by the RF model as

135 shown in Figure 4. Rn, which accounted for 78% and 76% of the total variable significance of H and LE, respectively, was the

136 most crucial variable in regulating the heat fluxes (Figures 4a and 4c). Consistent with the high variable significance values,

137 H and LE also had the highest r of 0.79 and 0.75 with H and LE, respectively, as shown in Figures 4b and 4d. The other four

138 factors contributed much smaller than Rn, and WS, T, RH, and P had importance values of 2%, 4%, 7%, and 5% (2.2%, 19%,

139 2%, and 0.6%) for H (LE), respectively. All these elements such as Rn, T, WS, RH are normalized before the model starts

140 training. When these elements are normalized, it ensures uniformity and comparability. In general, all of these predictors

141 played a role in the H and LE calculation, and for H, the sequence of importance was Rn, RH, P, T, and WS; while for LE, it

142 was Rn, T, WS, RH, and P. The most significant impact on the change of H and LE came from Rn, which was the most

143 important energy source of the surface and modulated the surface temperature directly. RH and T had a minor impact on the

144 H and LE changes in terms of climatic parameters, which carried the information of the light-dependent reactions of H and LE

145 fluxes. Particularly, WS and P had the minimal impacts on the H and LE fluxes. The WS, T, and RH also affected H and LE

146 according to the Monin-Obukhov similarity theory (Monin and Obukhov, 1954), while P represented the contributions from

147 the background weather systems.
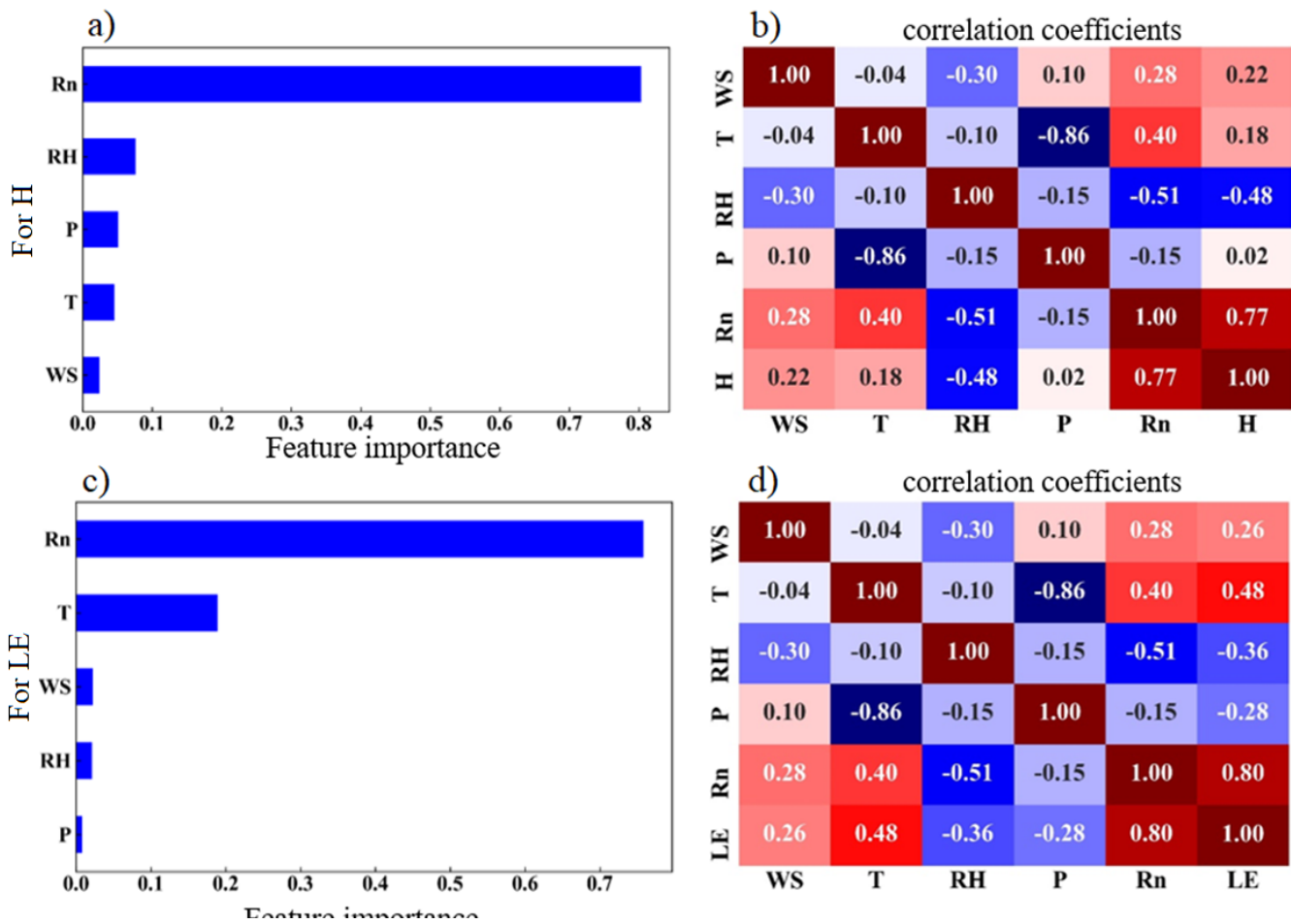
Figure 4. The feature importance of the variables for a) H and c) LE, and the correlation coefficient between each of the input variables for b) H and d) LE.

3.2 RF Model Evaluation

Figures 5-6 show the comparison between the observed and the RF-estimated H and LE, respectively. In the period of rice, the RF model showed good performance for both the training dataset (MAE =8.51 and 17.89 Wm^{-2}; RMSE =14.11 and 29.82 Wm^{-2}, for H and LE, respectively) and the testing dataset (MAE =9.61 and 10.34 Wm^{-2}, RMSE = 15.63 and 17.21Wm^{-2}, for H and LE, respectively) (Figures 5a, 5b, 6a, and 6b). RF model also showed high consistency with direct measurements for the validation dataset (MAE=5.88 and 20.97 Wm^{-2}, RMSE = 10.67 and 29.46 Wm^{-2}, for H and LE, respectively), (Figures 5c and 6c). In the period of wheat, the performance of the RF model for the training, testing, and validation datasets of H and LE was similar to that in the period of rice. For the training, testing, and validation datasets, respectively, the MAEs are 7.18, 8.01, and 6.01 Wm^{-2} for H, and 13.58, 8.82, and 19.93 Wm^{-2} for LE; and the RMSEs are12.27, 13.61, and 9.86 Wm^{-2} for H, and

161   24.92, 15.17, and 28.74 Wm^{-2} for LE (Figure 5d,e,f, Figure 6 d,e,f). These results demonstrate that the RF model is capable of

162   effectively calculating the H and LE with input variables of Rn, WS, T, RH, and P.
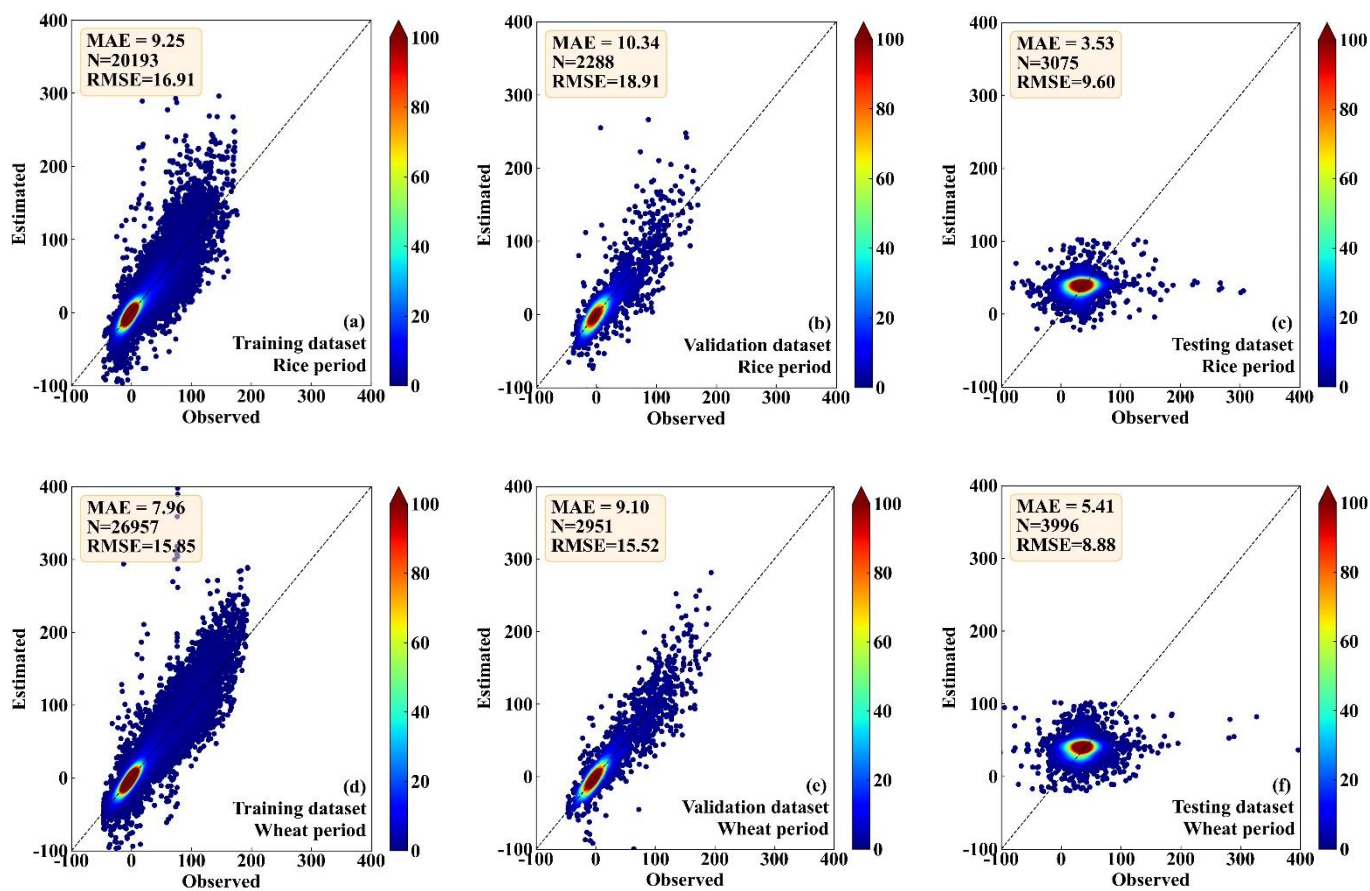
163

164   **Figure 5. Scatter density plots of the observed and the RF-estimated H values, a) and d) for the training dataset, b) and e) for the**

165   **validation dataset, and c) and f) for the testing dataset. And a), b) and c) are in the period of rice, while d), e) and f) are in the period**

166   **of wheat.**

167
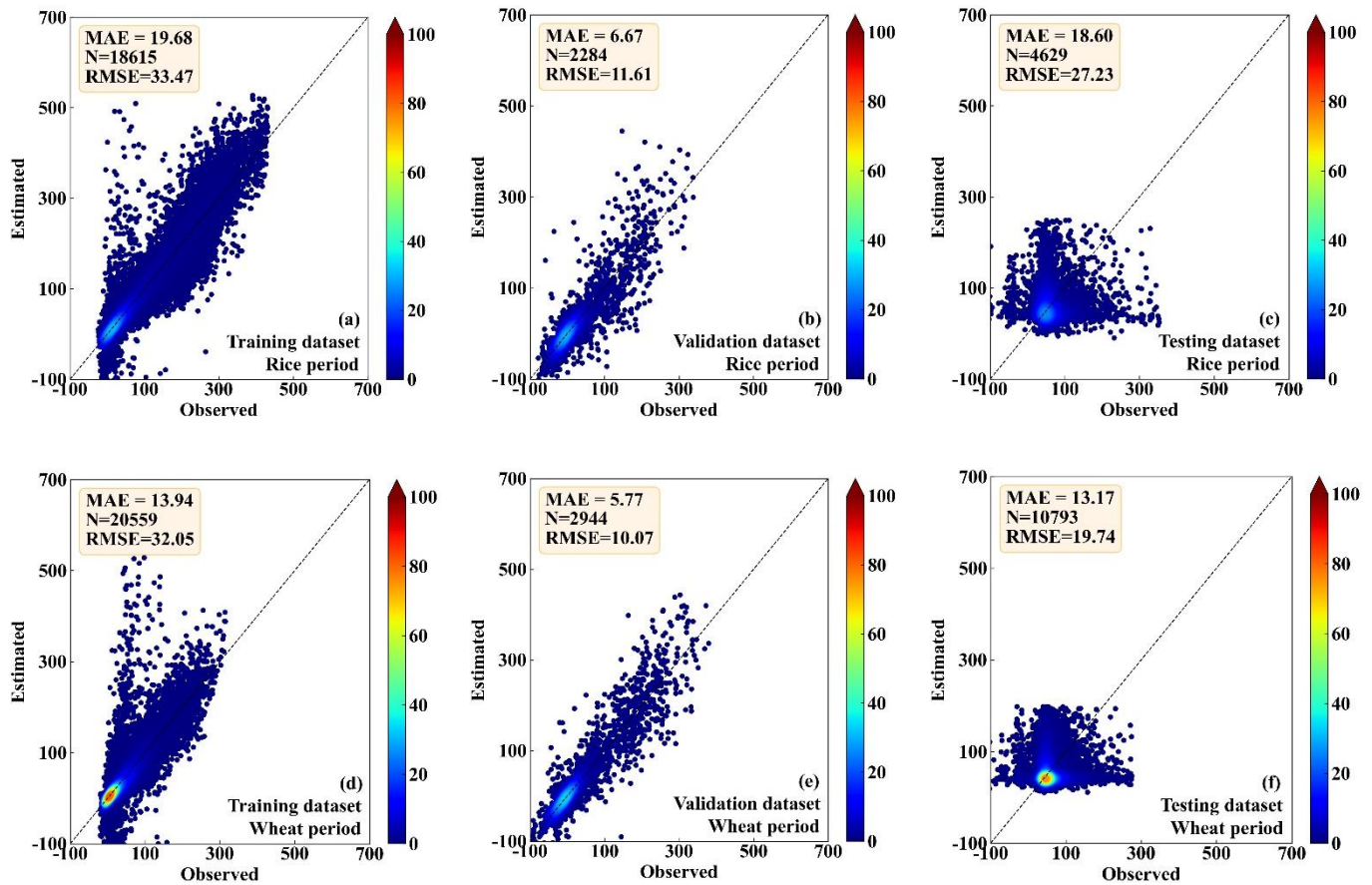
Figure 6. Same as Figure 5, but for LE.

3.3 Examination of Input Combinations

Meteorological elements may occasionally be unavailable due to the failure of sensors so the 5-variable input combination derived in Section 3.2 is not always applicable. Therefore, examination of other alternative input combinations is important to have substitute choices for data gap-filling when the 5-variable input combination is unavailable. In this subsection, we investigated the RF model's performance under the situation of lacking one element in the 5-variable input combination, i.e., we tested the 4-variable input combinations of (WS, T, RH, P), (Rn, T, RH, P), (Rn, WS, RH, P), (Rn, WS, T, P), and (Rn, WS, T, RH), by removing Rn, WS, T, RH, and P from the 5-variable input combination, respectively. The MAEs and RMSEs for these combinations are shown in Table 1, and it demonstrates that the RF model's accuracy may either increase or decrease as a result of the removal of a meteorological element during the training phase. For instance, it was found that the model's performance greatly improved once RH was eliminated from the input combination, with the MAE and RMSE of H decreasing from 6.48 and 11.94 Wm^{-2} to 5.66 and 11.06 Wm^{-2}, respectively, and LE from 19.1 and 39.39 Wm^{-2} to 17.74 and 35.27 Wm^{-2}. This outcome is logical given that RH and H do not have a strong correlation, as a result, performance will be enhanced if

RH is not included in the gap-filling processing pipeline. According to our findings, the RF model's performance may be greatly enhanced by excluding irrelevant meteorological elements from the study and choosing only those that have a significant impact on the variable. Our findings imply that in order to attain the best gap-filling accuracy, it is necessary to take into account both the advantages and disadvantages of ML-based models as well as the ideal input components.The results suggested that RH at a single level was not well correlated to the fluxes as shown in Section 3.1, because the one-level RH was strongly affected by the irrigation activity which was an external factor of the weather system. As a result, RF model performance was enhanced when the irrelevant variable (i.e., RH) was removed from the input list. The same condition also happened to the removal of WS, as could be seen from Section 3.1, WS showed small correlations with the fluxes. WS over this site was rather small, and frequently below 2 m s^{-1}, and under this light wind condition, the fluxes were mostly driven by the buoyancy rather than the wind shear. Figure 7 presents the MAE variation percentage of the 4-variable input combinations from the 5-variable input combination. After RH was removed from the input list, the RF model showed favorable performance for both H and LE, as shown in Figure 7, with MAE values improvements of 12.65 and 7.12%, respectively. Notably, the removal of Rn from the input combination resulted in a considerable decline in the RF model's performances, with MAE degradation percentage values reaching 16.20% and 10.73%, respectively. This outcome makes sense since Rn is highly associated with H and LE; hence, performance will be declined if Rn is left out of the input training dataset. As a consequence, our findings demonstrated that choosing strongly associated components could greatly increase the gap-filling accuracy. According to our findings, the best input combination is (Rn, WS, T, P).

Table 1.The MAEs and RMSEs of the RF-estimated heat fluxes for the 4-variable input combinations, and the corresponding changes from the 5-variable input combination.

Factors Included	Factors Eliminated		MAE (change)	RMSE (change)
WS, T, RH, P	Rn	H	7. 63 (+1. 15)	10. 72 (−1. 22)
		LE	21. 15 (+2. 05)	39. 38 (−4. 62)
Rn, T, RH, P	WS	H	6. 15 (−0. 33)	11. 42 (−0. 52)
		LE	18. 36 (−0. 74)	36. 13 (−2. 34)
Rn, WS, RH, P	T	H	6. 68 (+0. 20)	11. 48 (−0. 46)
		LE	19. 54 (+0. 44)	38. 54 (−1. 46)
Rn, WS, T, P	RH	H	5. 66 (−0. 82)	11. 06 (−0. 88)
		LE	17. 74 (−1. 36)	35. 27 (−4. 12)
Rn, WS, T, RH	P	H	6. 49 (+0. 03)	11. 77 (−0. 17)
		LE	19. 12 (+0. 02)	38. 13 (−1. 07)

203
204
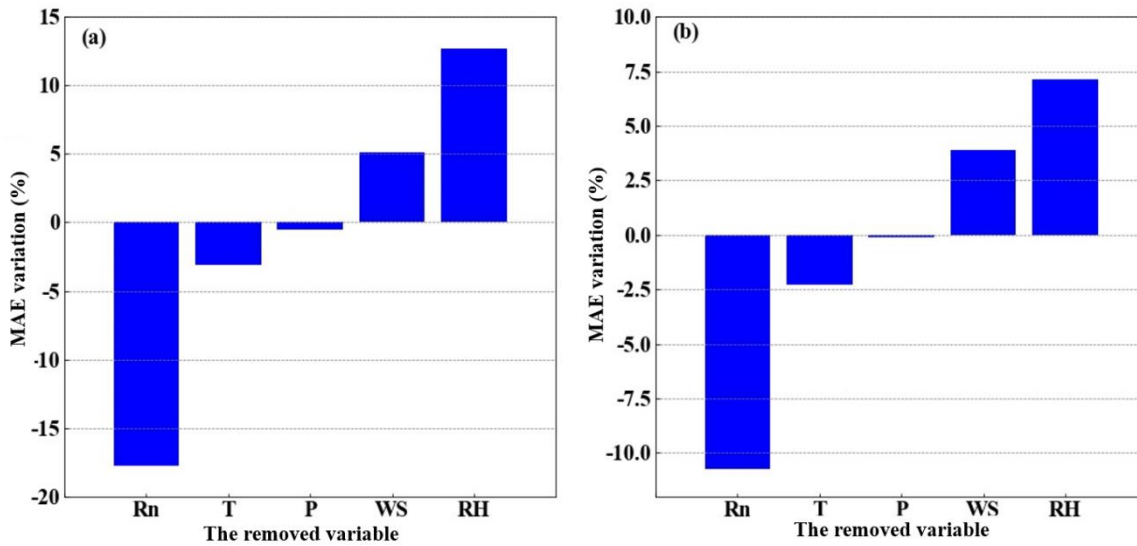
Figure 7. The MAE percentage variation after changing the 5-variable input combinations to the 4-variable input combinations, a)
for H, and b) for LE, respectively. The x-axis labels indicate the removed variables.

It should be noted that other variables that might have an impact on the H and LE were not investigated here. For example, given that our research site was over farmland and plants were growing, knowledge of the variations of the leaf area index (LAI) and inclusion of it to the training dataset should also be useful to increase the accuracy of the RF model in H and LE gap-filling. The monsoonal climate here also incurred considerable precipitation variations, which might as well potentially contribute to the RF model accuracy improvement. However, due to the lack of LAI and precipitation observations, the inclusion of the two variables into the RF model training dataset was not applicable in this study. Additionally, as shown above, more variables would bring a higher observation demand, and lead to more complexity and potentially decreased results, such as the adding variable of RH.

3.4 Comparison with other four ML methods

3.4.1 Comparison in H estimation

To further investigate the reliability of the RF model, we used a Taylor diagram to compare its performance in H estimation with other four ML models: support vector machine (SVM), k-nearest neighbor (KNN), gradient boosting decision tree (GBDT), and linear regression (LR). SVM is a data-oriented classification algorithm, and the basic model is to find the best separation hyperplane on the feature space so that the positive and negative sample intervals on the training set are maximum. Its advantages are that the kernel function can be used to map to a high-dimensional space; the use of the kernel function can

225 solve the nonlinear classification ; the classification idea is very simple, that is, to maximize the interval between the sample

226 and the decision-making surface ;the classification effect is better ;and the nonlinear relationship between data and features is

227 easy to obtain when the small and medium-sized sample size is large.KNN is particularly suitable for multi-classification

228 problems. Its advantage is that it is simple in thought, easy to understand, easy to implement; No estimation parameters, no

229 training; High accuracy, insensitive to outliers.GBDT can flexibly handle various types of data, including continuous and

230 discrete values. With relatively few parameter adjustment times, the prediction preparation rate can also be relatively high. If

231 the data dimension is high, the computational complexity of the algorithm will increase. Using some robust loss functions, the

232 robustness to outliers is very strong.LR is a statistical analysis method that uses regression analysis in mathematical statistics

233 to determine the quantitative relationship between two or more variables that depend on each other.The results have good

234 interpretability, can intuitively express the importance of each attribute in the prediction, and the calculation of entropy is not

235 complicated.

236 All the models were optimized with the same technique described above for the RF model. The results are shown in Figure 8.

237 The EC measurements were used as the benchmark. It can be seen that the RF model generally outperforms the other four

238 models, with the standard deviations (σ_n) and correlation values of 1.05 and 0.98 during the period of rice planting, and 0.96

239 and 0.95 during the period of wheat planting, respectively. The SVM model is the second most accurate model, with the σ_n and

240 correlation of 0.92 and 0.98 during the period of rice planting, and 0.91 and 0.93 during the period of wheat planting,

241 respectively. The LR model performs the worst, with the σ_n and correlation of 0.60 and 0.76 during the period of rice planting,

242 and 0.80 and 0.72 during the period of wheat planting, respectively. The accuracy of KNN and the GBDT models is in between

243 the above-discussed models, and the σ_n and correlation during the rice and wheat period for KNN are 0.68 and 0.73, and 0.77

244 and 0.82; and for GBDT are 0.79 and 0.80, and 0.81 and 0.9, respectively.

245
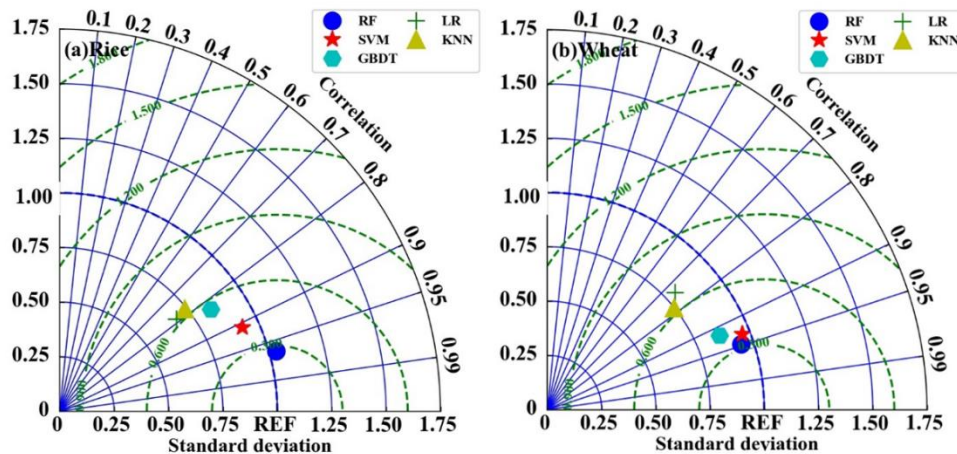
248 **Figure 8. The performances of the five models for estimating H in the period of a) rice and b) wheat.**

249

250 3.4.2 Comparison in LE estimation

251

252 Figure 9 illustrates a comparison of the estimated LE by all five models during the period of rice and wheat planting. The

253 results are similar to those in the H estimation, and the RF model is found to perform better than the other four models, with

254 the σ_n and correlation values of 0.95 and 0.97 during the period of rice planting, and 0.97 and 0.96 during the period of wheat

255 planting, respectively. Nonetheless, the KNN model performs the worse for LE estimating and has the σ_n and correlation

256 values of 0.68 and 0.82 during the period of rice planting, and 0.62 and 0.79 during the period of wheat planting, respectively.

257 Overall, as shown by the Taylor diagram of Figures 8 and 9, in this study the RF model has the best accuracy in either H or

258 LE estimation for data gap-filling.

259
260
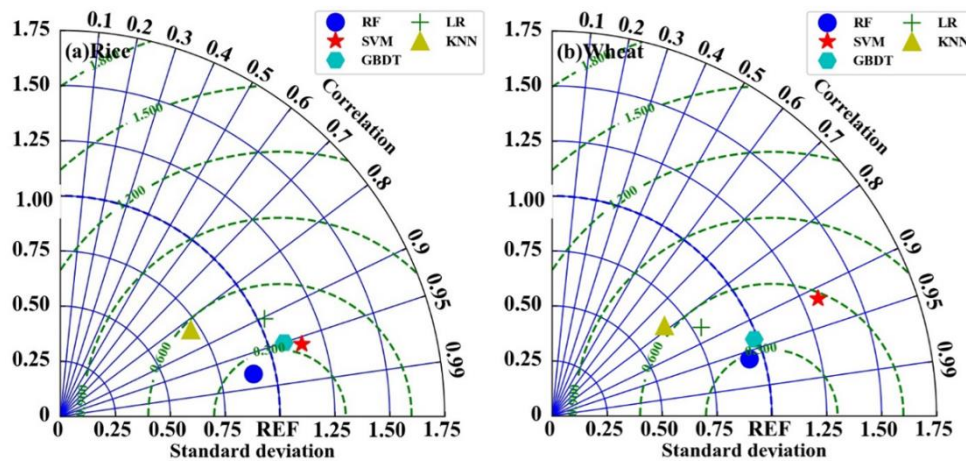
261 **Figure 9. Same as Figure 8, but for LE**

262

263 **4 Summary and Conclusions**

264 To assess the RF model's capacity for gap-filling the sensible and latent heat flux measurements over rice-wheat rotation

265 croplands, 90% of the total observation data gathered at Shouxian were utilized for training and testing, and the remaining 10%

266 for independent validation. Our findings demonstrate that Rn is the most important variable in regulating H and LE, and it

267 accounts for 78% and 76% of the total variable significance in the RF model construction for H and LE calculation, respectively.

268 The least important variables are WS and P, and their total variable significances are 2% and 0.6%, respectively. During the

269 periods of rice and wheat planting, the RF model with a 5-variable input combination shows reliable performance, with MAE

270 values of 5.88 Wm^{-2} and 20.97 Wm^{-2}, and RMSE values of 10.67 Wm^{-2} and 29.46 Wm^{-2}, respectively. However, further

271 analysis of the RF model with 4-variable input combinations indicates that the performance of the model is improved when

272 RH is removed from the input list, and the MAE values decrease by 12.65% and 7.12% for H and LE, respectively. Nonetheless,

273 the 4- variable input combination without Rn causes an increase in the MAE values of the model, by 16.20% and 10.73% for

274 H and LE, respectively. Therefore, the best input combination found in this study for heat fluxes gap-filling is (Rn, WS, T, P).

275 Statistical comparison of RF and other four typical ML models (LR, KNN, SVN, and GBDT) by Tylar diagram further shows

276 that RF is the most accurate, with the standard deviations and correlation values of 0.95 and 0.97 during the period of rice

277 planting, and 0.97 and 0.96 during the period of wheat planting, respectively. While the LR and KNN models perform the

278 worst for H and LE gap-filling, respectively, according to the statistical metrics of the Tylor diagram.

279

280 This study is based on only the data collected over rice–wheat-rotation croplands, but the method presented above to find a

281 reliable gap-filling ML model can also be used over other types of the underlying surface and in other climate zones. It should

282 be noted that over different types of the underlying surface and climates, the variable significances can vary and a careful

283 check of the input combinations is needed. For example, over polar oceans with strong winds, Rn probably is not the most

284 important driving factor, while the winds which cause mostly the turbulence may take the first place. On the other hand, over

285 areas without human irrigation activity, RH will possibly be strongly related to the latent heat flux, and hence the inclusion of

286 it into the input list may increase the ML model performance. Besides the examination of the input combinations, the choice

287 of an ML model and the method to optimize its parameters are also important.

288

289 Overall, this study shows the potential to use the RF model to produce trustworthy gap-filling data of H and LE over rice–

290 wheat-rotation croplands, and the ML methods are suggested to be used to derive the fluxes' estimations when direct EC

291 observations are not available.

292

293 *Data availability*. The data used in this paper is archived in Zenodo https://doi.org/10.5281/zenodo.7765608.

294

295 *Author contribution*. Jianbin Zhang: Methodology, Data analysis, Writing - original draft. Zexia Duand and Shaohui Zhou:

296 Methodology, Data analysis. Yubin Li and Zhiqiu Gao: Conceptualization, Writing - review &editing.

297

298 *Competing interests*. The contact author has declared that none of the authors has any competing interests.

299

300 *Acknowledgements*. The authors are grateful to the anonymous reviewers for their incisive comments.

301

302 *Financial support*. This study is supported by the National Natural Science Foundation of China (41875013).

303

References

Alavi, N., Warland, J.S., Berg, A.A.: Filling gaps in evapotranspiration measurements for water budget studies: Evaluation of a Kalman filtering approach, J. Agric. For. Meteorol., 141 (1), 57–66, https://doi.org/10.1016/j.agrformet.2006.09.011, 2006.

Anapalli, S.S.; Fisher, D.K.; Reddy, K.N.; Krutz, J.L.; Pinnamaneni, S.R.; Sui, R.: Quantifying water and CO_2 fluxes and water use efficiencies across irrigated C3 and C4 crops in a humid climate, J. Sci. Total Environ., 663, 338–350, https://doi.org/10.1016/j.scitotenv.2018.12.471, 2018.

Baareh, A.K.; Elsayad, A.; Al-Dhaifallah, M.: Recognition of splice-junction genetic sequences using random forest and Bayesian optimization, J. Multimed. Tools Appl., 80, 30505–30522, https://doi.org/10.1007/s11042-021-10944-7, 2021.

Belgiu, M.; Dragut, L.: Random forest in remote sensing: A review of applications and future directions, Isprs J. Photogramm. J.Remote Sensing., 114, 24–31, https://doi.org/10.1016/j.isprsjprs.2016.01.011, 2016.

Beringer, J., McHugh, I., Hutley, L. B., Isaac, P., and Kljun, N.: Technical note: Dynamic INtegrated Gap-filling and partitioning for OzFlux (DINGO), J. Biogeosciences., 14, 1457–1460, https://doi.org/10.5194/bg-14-1457-2017, 2017.

Best, M. J., M. Pryor, D. B. Clark, G. G. Rooney, et al.: The Joint UK Land Environment Simulator (JULES), model description - Part 1: Energy and water fluxes, J. Geosci. Model Dev., 4, 677-699, https://doi.org/10.5194/gmd-4-677-2011, 2011.

Bianco, M.J.; Gerstoft, P.; Traer, J.; Ozanich, E.; Roch, M.A.; Gannot, S.; Deledalle, C.-A.: Machine learning in acoustics: Theory and applications, J. Acoust. Soc. Am., 146, 3590–3628, https://doi.org/10.1121/1.5133944,2019.

Breiman, L.: Random Forests, J. Mach. Learn., 45, 5–32, https://doi.org/10.1023/A:1010933404324, 2001.

Cai, J.C.; Xu, K.; Zhu, Y.H.; Hu, F.; Li, L.H.: Prediction and analysis of net ecosystem carbon exchange based on gradient boosting regression and random forest, J. Appl. Energy., 262, 114566, https://doi.org/10.1016/j.apenergy.2020.114566, 2020.

Duan, Z.; Grimmond, C.; Gao, C.Y.; Sun, T.; Liu, C.; Wang, L.; Li, Y.; Gao, Z.: Seasonal and interannual variations in the surface energy fluxes of a rice–wheat rotation in Eastern China, J. Appl. Meteorol. Climatol., 60, 877–891, https://doi.org/10.1175/JAMC-D-20-0233.1, 2021.

Duan, Z.; Yang, Y.; Wang, L.; Liu, C.; Fan, S.; Chen, C.; Tong, Y.; Lin, X.; Gao, Z.: Temporal characteristics of carbon dioxide and ozone over a rural-cropland area in the Yangtze River Delta of eastern China, J. Sci. Total Environ., 757, e143750, https://doi.org/10.1016/j.scitotenv.2020.143750, 2021.

Falge, E.; Baldocchi, D.; Olson, R.; Anthoni, P.; Aubinet, M.; Bernhofer, C.; Burba, G.; Ceulemans, R.; Clement, R.; Dolman, H.: Gap filling strategies for defensible annual sums of net ecosystem exchange, J. Agric. For. Meteorol., 107, 43–69, https://doi.org/10.1016/S0168-1923(00)00225-2, 2001.

Foltýnová L.; Fischer, M.; McGloin, R.P.: Recommendations for gap-filling eddy covariance latent heat flux measurements using marginal distribution sampling, J. Theor. Appl. Climatol., 139, 677–688, https://doi.org/10.1007/s00704-019-02975-w, 2020.

337 Frazier, P.I.: A Tutorial on Bayesian Optimization, arXiv 2018, https://doi.org/10.48550/arXiv.1807.02811, 2018.

338 Gao, Z. Q., L. G. Bian, and X. J. Zhou.: Measurements of turbulent transfer in the near-surface layer over a rice paddy in China,
339   J. Geophys. Res., 108(D13), 4387–4387, https://doi.org/10.1029/2002JD002779, 2003.

340 Garratt, J. R.: The atmospheric boundary layer. Cambridge Atmospheric and Space Science Series, Cambridge University
341   Press, 316, https://doi.org/10.1017/CBO9781316117422, 2015.

342 Hui, D.; Wan, S.; Su, B.; Katul, G.; Monson, R.; Luo, Y.: Gap-filling missing data in eddy covariance measurements using
343   multiple imputation (MI) for annual estimations, J. Agric. For. Meteorol., 121, 93–111, https://doi.org/10.1016/S0168-
344   1923(03)00158-8, 2004.

345 Isaac, P., Cleverly, J., McHugh, I., Van Gorsel, E., Ewenz, C., and Beringer, J.: OzFlux data: Network integration from
346   collection to curation, J. Biogeosciences, 14, 2903–2928, https://doi.org/10.5194/bg-14-2903-2017, 2017.

347 Jiang, L.; Zhang, B.; Han, S.; Chen, H.; Wei, Z.: Upscaling evapotranspiration from the instantaneous to the daily time scale:
348   Assessing six methods including an optimized coefficient based on worldwide eddy covariance flux network, J. Hydrol.,
349   596, 126135, https://doi.org/10.1016/j.jhydrol.2021.126135, 2021.

350 Kepert, J.: Choosing a boundary layer parameterization for tropical cyclone modelling, J. Mon. Wea. Rev. [serial online].,
351   140(5), 1427-1445, DOI: https://doi.org/10.1175/MWR-D-11-00217.1, 2012.

352 Khan, M.S.; Jeon, S.B.; Jeong, M.H.: Gap-Filling Eddy Covariance Latent Heat Flux: Inter-Comparison of Four Machine
353   Learning Model Predictions and Uncertainties in Forest Ecosystem, J. Remote Sens., 13, 4976.
354   https://doi.org/10.3390/rs13244976, 2021.

355 Khan, M.S.; Liaqat, U.W.; Baik, J.; Choi, M.: Stand-alone uncertainty characterization of GLEAM, GLDAS and MOD16
356   evapotranspiration products using an extended triple collocation approach, J. Agric. For. Meteorol., 252, 256–268,
357   https://doi.org/10.1016/j.agrformet.2018.01.022, 2018.

358 Kim, Y.; Johnson, M.S.; Knox, S.H.; Black, T.A.; Dalmagro, H.J.; Kang, M.; Kim, J.; Baldocchi, D.: Gap-filling approaches
359   for eddy covariance methane fluxes: A comparison of three machine learning algorithms and a traditional method with
360   principal component analysis, J. Glob. Chang. Biol., 26, 1499–1518, https://doi.org/10.1111/gcb.14845, 2020.

361 Kunwor, S., Starr, G., Loescher, H. W., and Staudhammer, C. L.: Preserving the variance in imputed eddycovariance
362   measurements: Alternative methods for defensible gap filling, J. Agr. Forest Meteorol., 232, 635–649,
363   https://doi.org/10.1016/j.agrformet.2016.10.018, 2017.

364 Li, X., Z. Gao, Y. Li, and B. Tong.: Comparison of sensible heat fluxes measured by a large aperture scintillometer and eddy
365   covariance system over a heterogeneous farmland in East China, J. Atmosphere., 8, 101, https://doi.org/10.3390/
366   atmos8060101, 2017.

367 Liu, J.; Zuo, Y.; Wang, N.; Yuan, F.; Zhu, X.; Zhang, L.; Zhang, J.; Sun, Y.; Guo, Z.; Guo, Y.; et al.: Comparative Analysis
368   of Two Machine Learning Algorithms in Predicting Site-Level Net Ecosystem Exchange in Major Biomes, J. Remote
369   Sens., 13, 2242, https://doi.org/10.3390/rs13122242, 2021.

370 McCandless, T., Gagne, D. J., Kosović, B., Haupt, S. E., Yang, B., Becker, C., & Schreck, J. (2022). Machine Learning for
371   Improving Surface-Layer-Flux Estimates. Boundary-Layer Meteorology, 185(2), 199-228.

372 Moffat, A. M., Papale, D., Reichstein, M., Hollinger, D. Y., Richardson, A. D., Barr, A. G., Beckstein, C., Braswell, B. H.,
373   Churkin G., Desai, A. R., Falge, E., Gove, J. H., Heimann, M., Hui, D., Jarvis, A. J., Kattge, J., Noormets, A., and Stauch,
374   V. J.: Comprehensive comparison of gap-filling techniques for eddy covariance net carbon fluxes, J. Agr. Forest Meteorol.,
375   147, 209–232, https://doi.org/10.1016/j.agrformet.2007.08.011, 2007.

376 Moncrieff, J.; Clement, R.; Finnigan, J.; Meyers, T.: Averaging, Detrending, and Filtering of Eddy Covariance Time Series.
377   In Handbook of Micrometeorology: A Guide for Surface Flux Measurement and Analysis, The Netherlands, pp., 7–31,
378   https://doi.org/10.1007/1-4020-2265-4_2, 2006.

379 Monin, A. S., & Obukhov, A. M. (1954). Basic laws of turbulent mixing in the surface layer of the atmosphere. Contrib.
380   Geophys. Inst. Acad. Sci. USSR, 151(163), e187.

381 Nisa, Z.; Khan, M.S.; Govind, A.; Marchetti, M.; Lasserre, B.; Magliulo, E.; Manco, A.: Evaluation of SEBS, METRIC-
382   EEFlux, and QWaterModel Actual Evapotranspiration for a Mediterranean Cropping System in Southern Italy, J. Remote
383   Sens., 13, 4976 18 of 19, https://doi.org/10.3390/agronomy11020345, 2021.

384 Papale, D.; Reichstein, M.; Aubinet, M.; Canfora, E.; Bernhofer, C.; Kutsch, W.; Longdoz, B.; Rambal, S.; Valentini, R.;
385   Vesala, T.; et al.: Towards a standardized processing of Net Ecosystem Exchange measured with eddy covariance
386   technique: Algorithms and uncertainty estimation, J. Biogeosciences., 3, 571–583, https://doi.org/10.5194/bg-3-571-2006,
387   2006.

388 Reichstein, M.; Falge, E.; Baldocchi, D.; Papale, D.; Aubinet, M.; Berbigier, P.; Bernhofer, C.; Buchmann, N.; Gilmanov, T.;
389 Granier, A.; et al.: On the separation of net ecosystem exchange into assimilation and ecosystem respiration: Review and
390   improved algorithm, J. Glob. Change Biol., 11, 1424–1439, https://doi.org/10.1111/j.1365-2486.2005.001002.x, 2005.

391 Richard, A.; Fine, L.; Rozenstein, O.; Tanny, J.; Geist, M.; Pradalier, C.: Filling Gaps in Micro-Meteorological Data,
392   Switzerland, https://doi.org/10.1007/978-3-030-67670-4_7, 2020.

393 Stauch, V.J.; Jarvis, A.J.: A semi-parametric gap-filling model for eddy covariance CO2 flux time series data, J. Glob. Chang.
394   Biol., 12, 1707–1716, https://doi.org/10.1111/j.1365-2486.2006.01227.x, 2006.

395 Vitale, D., Bilancia, M., Papale, D.: A multiple imputation strategy for eddy covariance data, J. Environ. Inform., 34, 68–87,
396   https://doi.org/10.3808/jei.201800391, 2018.

397 Wang, L.; Wu, B.; Elnashar, A.; Zeng, H.; Zhu, W.; Yan, N.: Synthesizing a Regional Territorial Evapotranspiration Dataset
398   for Northern China, J. Remote Sens., 13, 1076, https://doi.org/10.3390/rs13061076, 2021.

399 Webb, E.K.; Pearman, G.I.; Leuning, R. Correction of flux measurements for density effects due to heat and water vapor
400 Transfer, Q. J. R. Meteorol. Soc., 106, 85–100, https://doi.org/10.1002/qj.49710644707, 1980.

401 Wilson, K.B.; Hanson, P.J.; Mulholland, P.J.; Baldocchi, D.D.; Wullschleger, S.D.: A comparison of methods for determining
402   forest evapotranspiration and its components: Sap-flow, soil water budget, eddy covariance and catchment water balance,
403   J. Agric. For. Meteorol., 106, 153–168, https://doi.org/10.1016/S0168-1923(00)00199-4, 2001.

404   Wutzler, T., Lucas-Moffat, A., Migliavacca, M., Knauer, J., Sickel, K., Sigut, L., Reichstein, M.: Basic and extensible post-
405   processing of eddy covariance flux data with REddyProc, J. Biogeosciences., 15 (16): 5015–5030,
406   https://doi.org/10.5194/bg-15-5015-2018, 2018.

407   Yu, T.C.; Fang, S.Y.; Chiu, H.S.; Hu, K.S.; Tai, P.H.Y.; Shen, C.C.F.; Sheng, H.: Pin accessibility prediction and optimization
408   with deep learning-based pin pattern recognition, J. IEEE Trans. Comput.-Aided Des. Integr. Circuits Syst., 40, 2345–
409   2356, https://doi.org/10.1145/3316781.3317882, 2019.